Comparison of Some Random-Barrier, Continuous-Time Random-Walk, and Other Models for the Analysis of Wide-Range Frequency Response of Ion-Conducting Materials

J. Ross Macdonald*

Department of Physics and Astronomy, University of North Carolina, Chapel Hill, North Carolina 27599-3255

Received: March 23, 2009; Revised Manuscript Received: May 24, 2009

Several theoretical models are fitted to an exact wide-frequency-range data set representing a new random-free-energy, effective-medium expression for mobile-ion response at low temperatures. A continuous-time, random-walk K1 model, indirectly involving a stretched-exponential temporal correlation function, led to the best fit, much superior to those of two dielectric-dispersion models as well. Two types of approaches are compared for analyzing $0.4Ca(NO_3)_2 \cdot 0.6KNO_3$ (CKN) experimental data covering a very wide frequency range: a simplified conventional approach, usually involving only some or all of the real part of conductivity, denoted type 1, and an approach involving nonlinear least-squares fitting of full complex data over its entire range, denoted type 2. The type-2 analysis uses a composite fitting model involving the K1 and involves 10 free parameters needed to well represent electrode polarization, conductive-system dispersion, nearly constant loss, and limiting far-infrared vibrational effects. It confirmed that the latter were purely dielectric and led to σ'' and ε'' boson peaks; included a mobile-charge explanation of the nearly constant loss region; and yielded reasonable values of the K1-model fractional exponent, β_1, and plausible values of a completely blocking double-layer capacitance. The good type-2 fit parameter estimates were used to generate extrapolated model response over a 20-decade range at complex conductivity and complex relative permittivity levels, as well as their accurate slopes over that range. The maximum slope of the log−log σ' curve failed to approximate well the value of 2 usually inferred from data of the present type but instead led to a novel double peak with peak slope values of about 1.6 and 1.7 before decreasing to zero at the limiting far-infrared plateau region of σ' response. Nearly constant loss was found to be well described by the series combination of the bulk high-frequency-limiting dielectric constant of the material and a translational ionic-motion constant-phase-element expression, one whose inclusion was also needed for representing low-frequency electrode polarization effects. Further, this combination should dominate the full response at sufficiently low temperatures.

1. Introduction and Background

In recent work, Schrøder and Dyre proposed an effective-medium approximation (EMA) to a random-free-energy barrier-hopping model (RBM) that yields an expression for its frequency response under extreme-disorder conditions (low-temperature limit).[1] In that work, the RBM was solved by a new approximate hopping model, here designated the MEMA, that involves the "fat percolation cluster", and it is stated that the MEMA provides "an accurate description of the universal ac conductivity". Here, the appropriateness of this description is examined in some detail.

Given that ref 1 provides much background information on ion conduction in disordered materials and mentions that the RBM well represents experimental conductivity data, it is worthwhile to compare the MEMA model with others, such as the Davidson−Cole (DCD, DC0, and DC1), KD, K0, and K1 models, that have proved useful in fitting and analyzing experimental data.[2−8] The KD, K0, and K1 models involve, directly or indirectly, a stretched-exponential (SE) temporal response. The DCD and KD approaches are appropriate for data involving dielectric dispersion, and the DC0, DC1, K0, and K1 approaches are appropriate for data involving dispersed ionic conduction. When a bulk dielectric constant, $\varepsilon_{D\infty}$, is included in a composite model involving DC1 or K1, it is designated by C in the composite model name; thus, for the K1 or DC1 model in parallel with such an element, the results are designated CK1 or CDC1. For other models, C denotes the total high-frequency-limiting dielectric constant ε_∞.

It is also pertinent to compare the MEMA response with that of relevant EDAE models, ones that are precursors of and alternatives to the MEMA model. Here, EDAE stands for an RBM model involving an exponential probability distribution of activation energies, a box distribution. In 1985, the present author published a comprehensive discussion of possible EDAE frequency-response models for both conductive and dielectric systems, including 3D complex-plane shapes and explicit formulas for a range of ψ parameter values.[9] This work involved a generalized box EDAE with the slope of its top boundary given by the parameter $\psi \equiv 1 - \phi$, with zero slope for $\psi = 0$. It was later generalized in ref 10, and the EDAE response was compared to that of a Gaussian distribution of activation energies (DAE) in ref 11.

Contemporaneously and independently, in 1985, Dyre published an article[12] based on a continuous-time, random-walk (CTRW) EMA model that led, after further approximation, to the $\psi = 0$ result of ref 9, a specific EDAE model. In 1988, he further discussed this model, then called the random free-energy barrier model,[13] and later, it was named the macroscopic percolation path approximation (PPA) model.[14] Finally, in 1989, in a work on conduction in disordered materials, the present author further discussed the utility of the PPA, some of the approximations leading to it, and its claim of universality.[15]

* Tel.: 919-967-5005. E-mail: macd@email.unc.edu.

10.1021/jp9026095 CCC: $40.75
Published on Web 06/15/2009

TABLE 1: LEVM CNLS Proportional-Weight Fits of a Normalized 1000-Point MEMA Data Set[1] with Various Fitting Models[a−d]

no.	model	$100S_F$	PDRMS	$\bar{\tau}_0$	fractional exponent	$\varepsilon_{C1\infty}$ or ε_∞	$\Delta\varepsilon$	ε_0	σ'' two slopes?; NFP
1	EDAE−PPA	45.7	0.014	0.313	1 F	0	0	0.156E	N; 1
2	EDAE	32.9	0.014	0.511	0.905	0	0	0.243	N; 2
3	K1	12.1	0.007	3.23×10^{-7}	0.880	6.48×10^{-3}C	0.932C	0.939E	Y; 2
4	RCKD	20.5	0.036	7.61	0.718	8.67×10^{-3}	0.991	1 E	Y; 3
5	RCEDAE	19.2	0.032	22.2	0.718	9.83×10^{-3}	0.990	1 E	N; 3

[a] Here, the letters F, C, E, NFP, Y, and N stand for fixed, calculated, extrapolated, number of free parameters, yes, and no, respectively. [b] The normalized dc conductivity, $\bar{\sigma}_0$, is fixed at 1 for all fits. [c] Rows 1−3 are conductive-system fits, and rows 4 and 5 are dielectric-system fits. [d] The high-frequency-limiting exponent of σ' is unity for the PPA and MEMA models; $\phi = 1 - \psi$ for the EDAE fits of rows 1, 2, and 5; $\phi = 1 - \beta_1$ for row 3; and $\phi = 1 - \beta_D$ for row 4, where ϕ is a free EDAE slope parameter.

The above background discussion indicates that the original EDAE and its successors contain a lot of physics, but it should be mentioned that the Dyre derivation of the PPA model involves a somewhat different CTRW approach than the one of Scher and Lax[16] that led to the specific K1 model.[4,17] The statement in ref 13 that the magnitude of the dc conductivity is usually quite wrong for the microscopic CTRW Scher−Lax model was earlier countered by them in ref 18, but it was not until 2002 that this model was generalized and shown to be made fully consistent by the addition of a high-frequency extension to it.[17] With the selection of a specific stretched-exponential temporal correlation function, it was then shown[17] to be isomorphic with a macroscopic K1 model of 1973.[19] An important article that appeared in 1989 compared theoretically and experimentally most of the important analysis models for conducting materials then existing,[20] and this work and refs 1 and 14 provide detailed analyses of the physicochemical content of many of the various models still competing for status in this area.

In section 2, exact wide-frequency-range MEMA data are fitted by a variety of its precursor models, by the K1 model, and by two dielectric-system dispersive models. Section 3 compares the efficacy of a simplified model and of a full model for fitting supercooled calcium potassium nitrate (CKN) over a 15-decade frequency range. Section 3.1 defines the two types of models, designated type 1 and type 2, and discusses exact and approximate log−log frequency-response slopes and the disadvantages of log−log plots of data and model responses. Section 3.2 deals with the alternatives of fitting data with conducting-system or dielectric-system dispersed response models, and section 3.3 discusses the results of full fits of CKN data at two temperatures using composite conducting-system models that include the K1. Section 3.4 uses the results of section 3.3 to present extrapolated, 20-decade, complex-conductivity frequency-response results for CKN at 342 K and their detailed slopes over the full range. Finally, section 3.5 compares and discusses various definitions for nearly constant loss as they apply to CKN.

2. Comparison of Model Predictions

The simplified $\psi = 0$ EDAE response model, the PPA, can be written in normalized form as

$$\sigma(\omega)/\sigma_0 \equiv \bar{\sigma} = i\bar{\omega}/\ln(1 + i\bar{\omega}) \qquad (1)$$

where σ_0 is the dc conductivity and $\bar{\omega} \equiv \omega\tau_\infty$. In ref 13, Dyre showed that the $\sigma'(\omega)$ predictions of eq 1 fitted several different experimental data sets reasonably satisfactorily, and in ref 15, the PPA was well fitted by a K0 model. The new MEMA expression[1] is given in normalized form by

$$\ln(\bar{\sigma}) = (i\bar{\omega}/\bar{\sigma})[1 + 2.66(i\bar{\omega}/\bar{\sigma})]^{-1/3} \qquad (2)$$

where here, $\bar{\omega} \equiv \omega\varepsilon_V\Delta\varepsilon/\sigma_0$, with ε_V as the permittivity of a vacuum.

It is noteworthy that both eqs 1 and 2 lead to fractional-exponent log−log slope values that reach unity at infinite frequency. At a finite specific frequency, it is the power-law slope at that frequency of a log−log representation of $\sigma'(\omega)$ or $\bar{\sigma}'(\bar{\omega})$. For simplicity, log−log slopes will be called just slopes hereafter.

Even though the MEMA conductivity data[1] extend to a normalized frequency of 10^{10}, transformation of the data to the dielectric level shows no finite-length high-frequency plateau for $\varepsilon'(\bar{\omega})$, although the magnitude of its slope continually decreases as the frequency increases. This suggests that the MEMA model might involve a nonzero ε_∞ value only in the infinite-frequency limit. Nevertheless, fitting this set with other models that include a nonzero ε_∞ value (represented by the letter C in the model name or an intrinsic part of the K1 model) leads to appreciably better fits than those without it. In the K1 model, a purely ionic effective dielectric quantity, $\varepsilon_{C1\infty}$, is present and is calculated from fit estimates of σ_0 and the mean value of the K1 characteristic relaxation time, τ_0.[4,17]

Table 1 summarizes the results of full complex-nonlinear-least-squares (CNLS) fits with proportional weighting, using the LEVM computer program,[21] of the MEMA data at the conductivity level for several different models. Not included are fit results for the CDC0 Davidson−Cole model and the CK0 model because these models led to fits as poor as or worse than that of the PPA model. Although no closed-form mathematical expression is available for the K1 model except for some values of its fractional exponent, β_1, such as $^1/_3$, $^1/_2$, $^2/_3$, and 1, the free LEVM program allows response values to be calculated for $0 < \beta_1 \leq 1$ for simulation and fitting. Its accuracy is greatest in the range $0.1 < \beta_1 < 0.9$. Fittings of data sets for many different materials involving a single mobile charge carrier using the K1 model have led to estimates of β_1 very close to $^1/_3$, nearly independent of temperature and mobile charge concentration.[3,4] When β_1 is fixed at this value, the K1 model is called the UN model, a semiuniversal one.

For the fits of rows 1−3, $\bar{\sigma}_0'$, the normalized dc conductivity, was fixed at unity. Further, the MEMA data involve an ε_0' value of unity as well. As the Table 1 results show, the model that fits the MEMA data best here is the K1, whose results are also shown in Figure 1. Note that the fractional-exponent slope value at a normalized frequency of 10^{10} is about 0.91 for the PPA

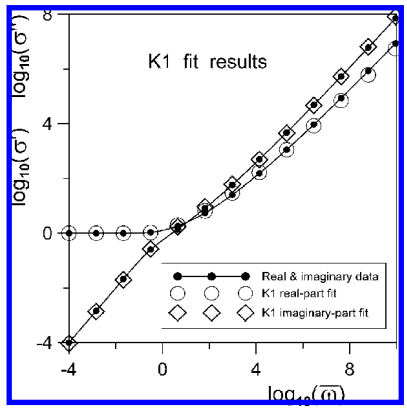

Figure 1. Log−log comparison of normalized MEMA conductivity data[1] with K1 model fit results. Only 13 fit points are shown for each curve. The best CNLS fit was found with the normalized dc conductivity fixed at unity, and the effective vacuum permittivity was also set to unity for transformation to other immittance levels.

model and 0.88 for the MEMA model, remarkably close to the values from the EDAE and K1 fit results, respectively.

For simplicity, Figure 1 shows only 13 of the 1000 MEMA data points. Note that, for perfect fits, the open symbols should enclose the small solid-data-point symbols entirely symmetrically.[8] The three highest-frequency $\bar{\sigma}'(\bar{\omega})$ K1-fit points deviate progressively from such perfection as the frequency increases. In addition, the row-3 K1-fit estimate of ε_0' is about 0.94 rather than the value of unity of the data. The log−log $\sigma''(\bar{\omega})$ data curve involves two nearly straight-line regions, with that at lower frequencies approaching a slope of unity in the zero-frequency limit. It is noteworthy that the EDAE models of rows 1, 2, and 5 involve only a single virtually straight line.

The composite dielectric-response models of lines 4 and 5 require a frequency-independent dc conductivity in parallel (denoted by R in the model name and here fixed at unity) and a free parallel ε_∞ parameter for adequate fitting. When model elements are written together in the model name, with no separation, the present convention requires them to be in parallel, but when they are in series, they will be separated by a • symbol. Thus, for the RCKD model, the R, C, and KD elements are all in parallel. The fit results presented in rows 4 and 5 are discussed in section 3.2.

When the MEMA data are restricted to their 644 lower-frequency points, a maximum normalized frequency of 10^5 is reached, together with a span of about 2.8 decades. One finds that fits of this data set with all models except the K1 model lead to $100S_F$ values about one-half of those for the full data set and to different parameter estimates, particularly to smaller fractional exponent estimates. In contrast, those for the K1 model remain very nearly the same, a highly significant result.

If an exact data set is fitted by a single model that is fully appropriate for it, so that no systematic or random errors are present, then fitting involving any non-zero-length part of the data will yield perfect fits with the same very well determined parameter estimates. Even for experimental data with random errors, such behavior will be well approximated if the proper fitting model is employed. We see from the results presented in Table 1 that the K1 model yields not only the smallest values of $100S_F$ but also much smaller values of PDRMS, the rms value of the relative standard deviations of the free parameters of a fit. Even though the K1 model does not fit the MEMA data well in the highest-frequency region, the present results show that it is indeed close to being a useful and practical surrogate for the MEMA model. This finding is valuable because the MEMA model is impractical for CNLS fitting of experimental data, whereas fitting with the CK1 model is straightforward using the free LEVM computer program.

3. Illustration of Real-World Fitting Problems

3.1. Aspects of Modeling and Analyzing Experimental Frequency-Response Data. Most experimental data are not measured at such low temperatures that the low-temperature limit modeled by the MEMA is necessarily a good approximation. In addition, within the usual experimental frequency-response data window, most $\sigma'(\omega)$ results increase by only two or three decades from their σ_0 dc values, and many of them involve a high-frequency-limiting slope very close to $^2/_3$, as in the UN model.[4,22] For data extending to terahertz frequencies, however, the slope can exceed $^2/_3$ and can reach values near 2 before a zero-slope plateau appears.[14,17]

Further, data that extend to low enough frequencies usually show significant electrode polarization effects involving partial or complete blocking of mobile ions, and it is then often found that a composite model involving a CUN and a series constant-phase element (SCPE), denoted here by the characters SC in a composite-model name and sometimes in earlier work by just S, usually leads to good fits over the entire available frequency region. CPE response, often associated with microscopically rough electrodes, can be expressed as $\sigma_{SC} \equiv \varepsilon_V A_{SC}(i\omega)^{\gamma_{SC}}$, with $0 < \gamma_{SC} \leq 2$, and it reduces to an ideal capacitance for $\gamma_{SC} = 1$,[22] a situation with no loss at all, either constant or variable.

In the literature, there are many references to slope values of 0, 1, and 2 for experimental frequency-response data, values often characterized as "exact". In fact, an ideal resistor can lead to an exact zero slope for $\sigma'(\omega)$, and an ideal capacitor involves a slope of exactly 1 for $\sigma''(\omega)$, both apparent for conductive-system Debye response (Db0), for which they are in parallel. Although such ideal elements do not exist in nature, deviations from their responses for real elements are usually small enough to neglect. Nevertheless, exact conductivity-slope values of 0, 1, and 2 are generally present for other models and for experimental data only as low- or high-frequency limiting values, as discussed below.

An example is provided by the dielectric Debye response model (DbD), one comprising a resistor and capacitor in series. For specific quantities, consider a frequency-independent real-part conductivity, σ_{Db}, in series with a frequency-independent relative permittivity, ε_{Db}, whose time constant is $\tau_{Db} \equiv \varepsilon_V \varepsilon_{Db}/\sigma_{Db}$. The corresponding Debye response at the conductivity level is then $\sigma_{SDb}(\omega) = \sigma_{Db}(i\omega\tau_{Db})/(1 + i\omega\tau_{Db})$, which leads to a high-frequency $\sigma'_{SDb}(\omega)$ plateau with a slope of zero at infinite frequency and to a slope approaching 2 for $\omega\tau_{Db} \ll 1$. Although the slope reaches 2 only at zero frequency, when $\omega\tau_{Db} < 0.1$, it will be difficult to distinguish the slope from 2.

There are two principal approaches to comparing data with a theoretical response model. In the first, designated type 1 here, one that is often employed to demonstrate the applicability of a model, the model is compared with data in the form $\sigma'(\omega)$, usually in a log−log plot, such as that part of Figure 1. In such cases, it is often not stated how the comparison was made, whether the real part of a CNLS fitting is being shown, or just an NLS fit result, or neither. Usually, numerical estimates of the values of the model parameters and their uncertainties are unmentioned, and no statistical measure of the fit quality is provided; rarely are other models used for fitting comparisons. It is often deemed adequate to demonstrate that the model data-point predictions are close to those of the data in the log−log plot, then usually termed a good or excellent fit.

However, log−log plots are noted for their ability to gloss over and hide small deviations, a defect somewhat ameliorated by the procedure used here in Figure 1.[8] Examples appear below. Further, presentation of a log−log $\sigma'(\omega)$ fit plot alone does not make it clear whether corresponding $\sigma''(\omega)$ fit results were also obtained from either a CNLS or NLS fit. If not CNLS, $\varepsilon(\omega)$ fits are unavailable to estimate dielectric parameter values. Finally, CNLS fitting of data by a plausible physical model that itself satisfies the Kronig−Kramers transform relations might allow one to assess whether the data also satisfy these relations when random errors are minimal. In summary, type-2 analyses use CNLS fitting; provide model parameter estimates and their uncertainties, measures of fit quality; and often include comparison of the adequacy of two or more models of interest, as in the present work.

3.2. The Maxwell Alternative. In a recent article, fits of a $0.35Li_2S\cdot0.65GeS_2$ 258 K data set were carried out to compare the appropriateness of fits with a conductive-system CUN·SC model and a dielectric-system RCKD·SC model.[23] This work also demonstrated the incorrectness of the use of the K1 model alone for data fitting, as in ref 19. The RCKD·SC model involves a nondispersed parallel dc resistivity associated with mobile ions (R); the usual parallel ε_∞ limiting dielectric constant (C); and the KD model, one involving a distribution of dielectric relaxation times.[6] Although it might seem strange to fit data usually taken to involve only dispersion arising from a distribution of resistivity relaxation times instead with an approach involving only dielectric dispersion, Maxwell's equations preclude discrimination between conductive and displacement currents by external measurements.[8,24] Further, the fits led to the large value of $\varepsilon_\infty \approx 42.6$, one that might involve ion pairs, structures that contribute little or no long-distance hopping response at constant temperature.

The above comparison showed that both dielectric and conductive composite models yielded good fitting results that varied very little with which of the four immittance levels was where fitting was carried out, an important criterion for appropriate models. Further, although the RCKD·SC fits led to slightly smaller S_F values, they involved two more free fitting parameters than did the conductive-system CUN·SC fit, and most important, the estimated relative standard deviations of two of the five RCKD·SC parameters were appreciably larger than those of any of the three CUN·SC ones. These results, although not conclusive, suggested that the assumption of resistivity dispersion was superior to that of dielectric dispersion for that data set. Table 1 presents a similar comparison between the K1-fit results of the MEMA data and the dielectric-system RCKD and RCEDAE fits of rows 4 and 5. Here, as expected, both the S_F and PDRMS results for the latter fits are much inferior to that using the K1 model.

3.3. Alternate Analyses of Very Wide Range CKN Data. Recently, two analyses of supercooled $0.4Ca(NO_3)_2\cdot0.6KNO_3$ (CKN) data sets have appeared in the literature.[7,25] Although I was unfortunately unaware of the analyses of ref 25 and its predecessors[26,27] when writing ref 7, the analyses of ref 7 are completely independent of the earlier work, thus involving both negative and positive features. The data sets used in the earlier works were generated by the group of Professor K. Funke, and those analyzed in ref 7 were kindly provided by Dr. P. Lunkenheimer. Both data sets involved a range of temperatures above $T_g \approx 333$ K, and special attention and analysis were devoted to the 353 K results of ref 25 and to the 342 K results of ref 7. Here, we thus compare some of the type-1 353 K analysis results with updates of the type-2 342 and 361 K results

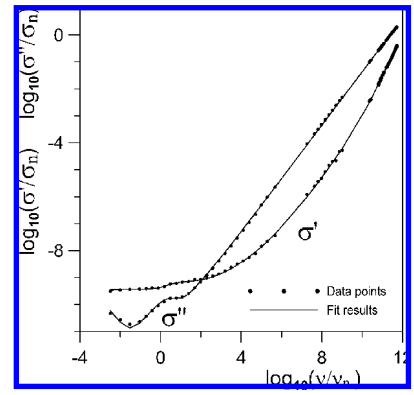

Figure 2. Log−log plots of real and imaginary 342 K CKN conductivity data parts versus frequency compared with the composite model-B CNLS fit results summarized in Table 2. Here and elsewhere, σ_n is 1 S/cm, and ν_n is 1 Hz.

of ref 7. Although the identity of the mobile ions in CKN was not discussed in ref 25, earlier work cited in ref 7 identified those with the largest mobilities as NO_3^- and K^+, with dynamical heterogeneity present.

Figure 2 shows the results at the conductivity level of a type-2 fit of the nearly 15 decade 342 K data set, and specific fit results are summarized in Table 2. Two slightly different composite models were used for fitting, with these models defined in the Table 2 footnote. Many parameters are needed in such models in order to properly represent the many physicochemical processes present in such an extended data set. Model B, expressed by $[C(R_i\cdot K1)]\cdot[G_P(SC\cdot R_{pl})\cdot C_S]$, is a simplification and improvement of the model used in ref 7 (10 free parameters here rather than 11). Because only wide-range resistivity- and electric-modulus-level plots were included in ref 7, here, we concentrate on complex conductivity and relative permittivity plots. For simplicity, the symbols in the names of models A and B are expressed in terms of resistors, capacitors, and fitting models, but they are explicitly defined in specific form in column 3 of Table 2.

The full meaning of the model-B name is a capacitance C in parallel with the series combination of a resistor R_i and the K1 fit model, all in series with a conductance G_P, itself in parallel with the series combination of the SC CPE model and a plateau resistance R_{pl}, and finally a blocking capacitance C_S in series with the rest of the model. Model A differs from model B only in its Debye DbD element, one that represents vibrational effects above about 10 GHz and leads to a high-frequency-limiting plateau in σ'. The series elements C_{Db} and R_{Db} of model A are closely equivalent to the model-B C ($\varepsilon_{D\infty}$) and R_{pl} elements, but the placement in model B of this resistance differs from that in model A.

Because the PDRMS value obtained from model-B fitting is appreciably better than that obtained with model A, we deal only with the latter. Note that the epsilon estimates of rows 9−12 of Table 2 are those of the model without any electrode contributions. Thus, $\varepsilon_\infty = \varepsilon_{C1\infty} + \varepsilon_{D\infty}$, and $\varepsilon_0 = \varepsilon_{C10} + \varepsilon_{D\infty}$. The main electrode polarization elements of models A and B are those denoted by SC and C_S.

If we specify values of the statistical fit measures S_F and PDRMS in the form S/P, then for model-B fits with the usual K1 model or with the K1 model replaced by the DC1, DC0, or EDAE, one finds the values 0.045/0.026, 0.056/0.045, 0.085/0.064, and 0.084/0.047, respectively. These results demonstrate the superiority of the present model-B choice involving dispersive K1 response. Its S_F value of 0.045 is satisfactory for a fit covering nearly 15 decades of relatively noisy data.

TABLE 2: LEVM CNLS Proportional-Weight Fit Results of CKN Data[a]

no.	fit quality measures and model parameters	actual parameter symbols	model A	model B	
			$T = 342$ K	$T = 342$ K	$T = 361$ K
1	s_F	−	0.0449	0.0448	0.0363
2	PDRMS	−	0.0486	0.0259	0.0421
3	C_{Db} or C	ε_{Db} or $\varepsilon_{D\infty}$	8.166|0.004	8.210|0.004	8.665|0.005
4	R_{Db}	ρ_{Db}, Ω-cm	0.0772|0.013	−	−
5	R_i	ρ_i, Ω-cm	24.30|0.092	26.68|0.048	3.053|0.077
6	K1	ρ_{C10}, Ω-cm	1.37×10^9|0.014	1.37×10^9|0.014	1.19×10^6|0.010
7	K1	τ_{C10}, s	6.18×10^{-6}|0.102	4.86×10^{-6}| $< 10^{-4}$	1.44×10^{-8}|0.035
8	K1	β_1	0.294|0.016	0.286|0.005	0.319| $< 10^{-4}$
9	K1, calc	$\varepsilon_{C1\infty}$	0.519	0.467	0.969
10	K1, calc	ε_{C10}	8.470	8.722	11.43
11	model	ε_∞	8.685	8.677	9.634
12	model	ε_0	16.64	16.93	20.10
13	G_P	σ_P, S/cm	7.18×10^{-10}|0.027	7.20×10^{-10}|0.027	3.78×10^{-6}|0.028
14	R_{pl}	ρ_{pl}, Ω-cm	−	0.0769|0.009	0.0345|0.030
15	SC	A_{SC}	1.35×10^3|0.040	1.36×10^3|0.039	1.02×10^5|0.083
16	SC	γ_{SC}	0.891|0.002	0.891|0.002	0.720|0.004
17	C_S	$\varepsilon_S \equiv C_S/\varepsilon_V$	1.21×10^6|0.044	1.21×10^6|0.044	8.43×10^5|0.043

[a] Nomenclature: AB indicates circuit elements A and B in parallel, and A·B denotes those elements in series. P|U designates a parameter value and its relative standard deviation (RSD) uncertainty. Model A is represented by $[(R_i \cdot K1)DbD] \cdot [G_P SC) \cdot C_S]$; model B is represented by $[C(R_i \cdot K1)] \cdot [G_P(SC \cdot R_{pl}) \cdot C_S]$. S_F is the RSD of fit residuals, and PDRMS is the rms value of the RSDs of the free fit parameters. The dielectric Debye model (DbD) here involves $C_{Db} \cdot R_{Db}$.

It is of interest to compare the results of replacing the K1 expression in model B with the UN one, where β_1 is fixed at $^1/_3$. For the 342 and 361 K data sets, the S/P results are 0.048/0.035 and 0.036/0.044, respectively. Because the 361 K β_1 estimate is already very close to $^1/_3$ with the K1 model, its UN fit results are little changed, with a slightly smaller $\varepsilon_{C1\infty}$ estimate of 0.965. For the 342 K data, however, the replacement leads to an appreciably larger estimate of τ_{C10} and to the much larger $\varepsilon_{C1\infty}$ value of 8.77, emphasizing the greater appropriateness of the K1 choice for this temperature.

Incidentally, in refs 25 and 26, it is stated that the CKN data sets presented there are consistent with those of Lunkenheimer and his group, the ones used here.[7] In fact, however, the 343 K[27] and 353 K[25,27] $\sigma'(\omega)$ data plots show no trace of the relatively small jog apparent at about 1 Hz in the corresponding Figure 2data curve. It is associated with the G_P (σ_P) term in the model, one comparable in size to the K1-model dc conductivity $\sigma_{C10} = 1/\rho_{C10}$. Although the jog is invisible in a log−log plot of the present 361 K data (not included here), Table 2 shows that σ_P is still well determined at that temperature. There is no analog of this quantity in the modeling approach of ref 25. Unlike the present analysis, that of ref 25 includes no account of electrode polarization and no plots of $\sigma''(\omega)$. As demonstrated in Figure 2, such effects are much more evident in $\sigma''(\omega)$ log−log response curves than in $\sigma'(\omega)$ ones. Further, as discussed in the following section, they can play a role not only at low frequencies but in modeling at higher frequencies as well.[28]

It is significant that, for the present 342 K CKN data set, involving a $\sigma'(\omega)/\sigma_0$ span of more than nine decades, a CK1 fit of a limited-range, modulus-level part of it, extending a few decades beyond the peak of its M'' response, led to a β_1 estimate of only about 0.16,[7] reminiscent of the row-3 K1 fit of MEMA data shown in Table 1. However, the present Table 2 fits of the full data sets involve very well determined estimates of β_1 of about 0.29 for 342 K and increasing to about 0.32 at 361 K, nearly the UN value of $^1/_3$. The approach toward $^1/_3$ at higher temperatures might be a consequence of changes in microscopic heterogeneity. These results suggest that, when fits of limited-range experimental data yield β_1 estimates below about 0.2, such values should be suspect and not necessarily related to the extreme-disorder RBM behavior described by the MEMA model.

The main part of the ref-25 analysis model is termed the MIGRATION concept (MC). Here, MIGRATION stands for "mismatch-generated relaxation for the accommodation and transport of ions". Like nearly all conductive-system models, it involves both forward and backward hopping.[29] Also, like RBM models, in the absence of a high-frequency plateau, it leads to a σ' slope that reaches a limiting infinite-frequency value of 1. Usually, however, it involves an approach to a zero-slope plateau.

It is interesting that the 353 K log−log type-1 $\sigma'(\omega)$ MC approach shown in Figure 4a of ref 25 appears good up to nearly 10 GHz, the end of the hopping part of the data, equivalent to the part up to about 1 GHz in the present plot of Figure 2. The higher frequency part of the data in Figure 4a of ref 25, identified as vibrational response, appears to be fitted there by a line of slope 2. Finally, although it is concluded in ref 25 that no NCL behavior is present in CKN, for some other materials it was found necessary to add to the MC a nontranslational empirical expression with slope near 1 to represent the data between its vibrational segment and hopping region.[27,30] These results and conclusions are further discussed in the next section.

All analysis models are necessarily idealized and thus approximate. In addition, there are empirical elements in both the MEMA and MC models. Although the extended Scher−Lax CTRW model, in the form of the K1,[17] is a Hartree approximation to the RBM, as already mentioned, it has, perhaps uniquely, been derived by both macroscopic and microscopic approaches,[17,19] and it has also been found to fit data for a wide variety of materials better than other models in type-2 fits.

Because the K1 and UN theoretical models have been found to be so generally applicable for disordered solids and even single crystals and supercooled liquids, it is worth mentioning that they involve diffusion in a medium with randomly distributed static trapping sites. Although the original 1973 microscopic Scher−Lax model[16] involves a general correlation function not specified there to be of SE form, an SE was a part of the 1973 modulus-formalism macroscopic model[19] and was

first introduced into the extended CTRW Scher−Lax model in 2002, thus making it isomorphic with the macroscopic K1 one.[17] Meanwhile, in 1982, Grassberger and Procaccia showed that, for diffusion in a medium with randomly disordered static traps, asymptotic temporal SE behavior appeared with a β exponent given by $d^*/(d^* + 2)$, where d^* is the dimension of the configuration space in which diffusion occurs.[31] Finally, this same result, applied to the K1 model, was shown in 2005 to be a simple consequence of topological constraint theory.[4,32]

As mentioned in ref 25, conductive-system data sets for many materials have been found to satisfy a time−temperature superposition principle that implies a temperature-independent shape, mechanism, or model in the frequency domain. In the hopping regime before any high-frequency plateau becomes apparent, when the UN model is found to fit the data well, it satisfies this requirement, and in addition, it is independent of mobile-ion concentration over a wide range.[3,4] Because CKN undergoes an Arrhenius-to-fragile shape transition around 375 K,[25,26] the MC model does not directly satisfy time−temperature superposition over the full range from just above T_g to 393 K.

There is one parameter discussed in ref 25 common to both MC and K1 fits, namely, ε_∞. For the 353 K data set, its lower and upper limits are stated to be 9.75 and 10.5. If one makes the reasonable assumption that a linear interpolation between the 342 and 361 K estimates of ε_∞ listed in Table 2 is adequate, one finds a value of about 9.23 at 353 K, somewhat below the lower limit above, but probably more accurate than it.

Yet, the matter is actually more complicated here. The present models include no n^2 limit for $\varepsilon_{D\infty}$, and thus, at sufficiently high frequencies, that part of $\varepsilon'(\omega)$ associated with $\varepsilon_{D\infty}$ begins to decrease toward zero with a time constant of $\tau_{pl} \equiv \varepsilon_V \varepsilon_{D\infty} \rho_{pl}$. Similarly, the $\varepsilon_{C1\infty}$ contribution to $\varepsilon'(\omega)$ begins to decrease with a time constant of $\tau_{C1\infty} \equiv \varepsilon_V \varepsilon_{C1\infty} \rho_I$. For the 361 K data of Table 2, the frequencies corresponding to these quantities, $\nu_{C1\infty}$ and ν_{pl}, are about 6.0×10^{11} and 6.1×10^{12} Hz, respectively, whereas for the 342 K data, they are about 1.4×10^{11} and 2.8×10^{12} Hz. Thus, $\varepsilon_\infty = \varepsilon_{C1\infty} + \varepsilon_{D\infty}$ first begins to decrease, and then a decade higher, the contribution of ε_∞ decreases as well.

These results clearly demonstrate that the so-called vibrational response that leads to the plateau in $\sigma'(\omega)$ and to its low-frequency flank with a slope near 2 involves dielectric Debye response leading to the above expression for τ_{pl}, with $\varepsilon_{D\infty}$ and ρ_{pl} in series. Thus, it properly does not involve ε_∞, a quantity that includes ionic effects when $\varepsilon_{C1\infty}$ is nonzero. Here, $\varepsilon_{D\infty}$ is a purely dielectric quantity closely proportional to temperature and probably involving induced dipoles but not ions or even ion pairs. In contrast, the thermally activated quantity $\sigma_{pl} \equiv 1/\rho_{pl}$ is exactly the final $\sigma'(\omega)$ plateau value. In ref 33, the authors consider disorder-induced far-infrared absorption in amorphous materials, a citation used in ref 25 to justify a slope of exactly 2 on the low-frequency flank, although it was specified as ≤ 2 in ref 33. Further, they found that the flank response was temperature independent for most amorphous materials studied, not exactly the situation here for a supercooled liquid. They also suggested that their real-part conductivity data involved vibrational (possibly phonon) modes. The increase of both $\varepsilon_{D\infty}$ and σ_{pl} with increasing temperature possibly suggests a corresponding increase in the number of effective modes.

Because Arrhenius behavior was found for the temperature range of the present data,[25] we can use the 342 and 361 K results listed in Table 2 to obtain preliminary approximate estimates of activation energies. For ρ_{C10}/T, τ_{C10}, $\langle\tau_{C10}\rangle$, ρ_i, ρ_P, ρ_{pl}, A_{SC}, and $T\varepsilon_{C1\infty}$, one obtains the following activation energies in electronvolts: 4.26, 3.26, 3.79, 1.19, 5.14, 0.44, −2.38, and −0.33, respectively. Although the series quantities ρ_{C10} and ρ_P are somewhat comparable in size, the appreciable difference in their estimated activation energies suggests that they might involve mobile charge species in different ways.

Because ρ_{C10} is so much larger than ρ_i here, the expression for $T\varepsilon_{C1\infty}$ that includes $\Delta\rho$ (ref 6, eq 6) reduces here to the usual expression

$$T\varepsilon_{C1\infty} = (\langle\tau_{C10}\rangle/\varepsilon_V)/(\rho_{C10}/T) \quad (3)$$

with high accuracy, where $\langle\tau_{C10}\rangle \equiv [\tau_{C10}/\beta_1]\Gamma(1/\beta_1)$ and Γ is the Euler gamma function. In many thermally activated situations with a single species of mobile charge, one finds that the two temperature-dependent terms on the right side of eq 3 have equal activation energies and then $T\varepsilon_{C1\infty}$ is not thermally activated and depends directly on the mobile charge density, nearly temperature independent if fully dissociated. Here, however, with two or more species of mobile charge, $T\varepsilon_{C1\infty}$ exhibits an activation energy about equal to the difference between those of eq 3 within their likely uncertainties.

A final anomaly is the relatively large decrease in the blocking specific capacitance, C_S, with increasing temperature apparent in Table 2. Its model-B value is about 0.1 μF/cm, not unreasonable for a double layer. Simple double-layer capacitance is proportional to the square root of the mobile charge number divided by the absolute temperature. The decrease associated with the direct change from 342 to 361 K amounts to only a factor of about 0.97, leaving a factor of about 0.5 to be explained if the remainder is attributed to a decrease of mobile charge. Although many more complex expressions for double-layer effects are available (e.g., ref 34), they do not lend credence to such a decrease.

3.4. Extended-Range 342 K CKN Responses and Slopes. The results in Table 2 and the discussion in section 3.3 illustrate how much more can be learned from a full type-2 data analysis than from a conventional type-1 approach. However, even when a good type-2 fit of an available data set has been obtained, there is still more to be learned. A CNLS fit of data filters and smoothes noise; thus, the fit model and its estimated parameters can be used with a new extended-range data set to calculate the exact response of the model over a wider extrapolated range.

Although all extrapolation is necessarily somewhat uncertain, extrapolation a few decades beyond the original data range at both ends can lead to new insights about responses intrinsic in the model, and probably in the data as well, ones not evident for the original data range. Further, because of the smoothing effect of model fitting, one can readily calculate the associated slope response over the new range even when the original data, such as the present CKN data sets, are noisy and preclude meaningful slope calculation by point-to-point numerical differentiation. Slope results are shown in Figure A.4 of ref 35, and derivatives of the data were employed for slope and parameter estimation in ref 36.

Figure 3 shows exact, extrapolated model-B 342 K CKN σ' log−log frequency response over the range from 10^{-5} to 10^{15} Hz compared to the limited-range original data points. The extended-range data involved 10 points/decade. In addition to the full model response, those of various parts of the full composite fitting model are included in the figure as well. In particular, we see that addition of the series R_i parameter to the CK1 model leads to a response region with a slope approaching 2 until a plateau is reached.[17] Further, the full model without the series R_i and R_{pl} resistive parameters leads to excellent agreement with the data up to about 1 GHz, thus including the

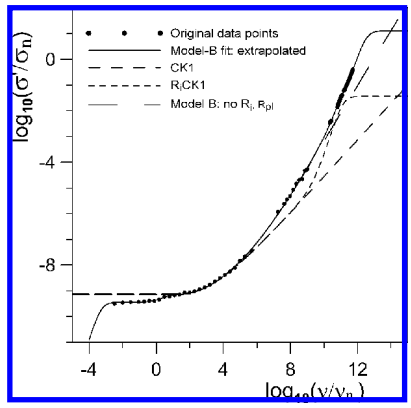

Figure 3. Log−log plot of exact σ' frequency response calculated from the parameter values of the model-B fit of 342 K CKN data over an extended frequency range of 20 decades. The original data points are included, as well as the individual responses of various parts of the full model.

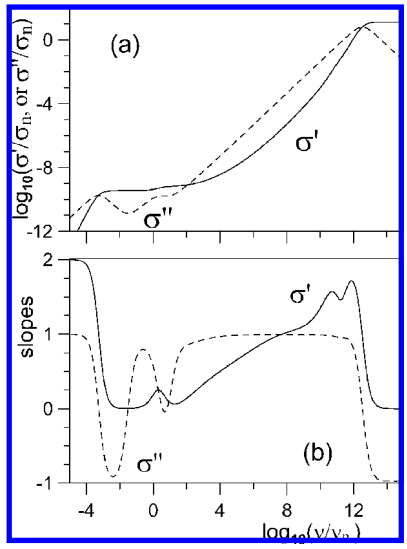

Figure 4. (a) Log−log plots of exact extended-range real and imaginary model-B 342 K CKN conductivity responses versus frequency. (b) Slopes calculated from the results in part a.

region between about 10^7 and 10^9 Hz with an apparent slope near 1. This response is dominated by SC-model contributions and is further discussed in the next section.

Comparison in Figure 3 of the extended-range response with the original data points shows nothing surprising except possibly the difference between the R_iCK1 and full-model high-frequency plateau positions. A similar plateau response appeared for the MC-model 353 K CKN fit.[25] Nevertheless, slope calculation leads to some unanticipated results.

Figures 4 and 5 show full extended-range results for both complex conductivity and relative permittivity and for their calculated slopes. Because the original data points were included in some of the earlier graphs, they are also shown in Figure 5a. Although the slope results of Figures 4b and 5b are very similar and related by a simple equation, they are both included here to show limiting low- and high-frequency results. Note that the ε'' peak appearing at about 7 THz in Figure 5a is similar to those for some other materials in the present frequency range that have been identified as boson peaks.[7] Such peaks in vibrational spectra were ascribed by Elliott to phonon scattering caused by intrinsic density-fluctuation domains in amorphous materials.[37]

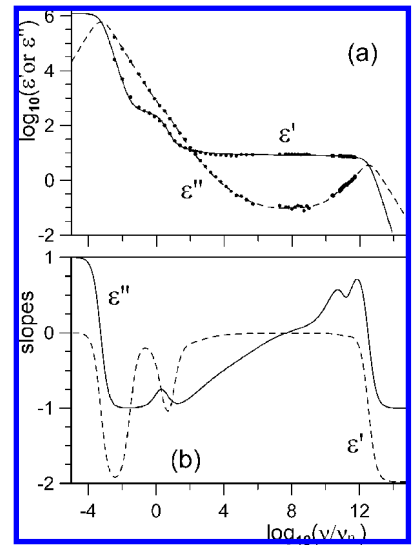

Figure 5. (a) Log−log plots of exact extended-range real and imaginary model-B 342 K CKN dielectric constant responses versus frequency. (b) Slopes calculated from the results in part a.

Unexpected results appearing in Figure 4b are that the σ' slope in the region from about 10 GHz to 1 THz fails significantly to approximate the exact slope of 2 used in ref 25, and in addition, there are two peak values in the slope before it begins to decrease toward its zero plateau value. Evidently, the log−log σ' curves of Figures 2 and 3 have too little resolution to provide a hint of such behavior. This is because the width of the data-point line in this region is determined by the scatter in the positions of the points, not primarily by their plotted size. The two peak slope values are about 1.57 and 1.72 at frequencies of 5.3×10^{10} and 7.5×10^{11} Hz, respectively. They are not associated with the use of a limited number of points because exactly the same results were obtained with data involving 40 points/decade.

We see from Figure 5b that the same double-peak slope behavior is apparent for the dielectric loss response as well. Very similar results, with somewhat smaller peak slope values, are also present for the present 361 K data. Even though ε'' boson peaks have been observed before, no slope calculations of the present type have been included for the frequency region of such peaks; thus, it must remain somewhat uncertain whether the present double peak is real and possibly involves more than a single type of phonon states, or whether it is an artifact associated with the present composite fitting model and/or recalcitrant scatter in the data. The presence of the double peak for both temperatures seems to make it more likely, however, that it is an inherent characteristic of CKN response.

3.5. Nearly Constant Loss Possibilities in CKN. Although early work[38] identified constant loss as a region of ε'' independent of frequency and thus corresponding to a slope of 1 for the same region of σ', when it was realized that such loss is physically impossible for a dispersive response model,[39,40] it was thenceforth usually called nearly constant loss (NCL) and often observed in the low-temperature region of the behavior of a particular material.[3,5,22,28,39−42] A more restrictive definition of NCL[25] is discussed below, and a recent summary of some of its possible origins appears in ref 43. NCL is important because its genesis has been the subject of much study and speculation, and its eventual resolution can therefore shed valuable light on material properties and behavior. One common explanation is that NCL involves the limited motion of ions at high frequencies caged by potential barriers where few if any ions escape the cage to hop. Some earlier summaries of work on NCL appear

in refs 25, 40, and 42, and in ref 42, it is suggested that NCL involves contributions from coupled ionic and dielectric processes and can thus involve interactions between vibrating or hopping ions and dipoles of the bulk material.

For the 342 K CKN data and model-B fit, Figure 5a shows an ε'' NCL region of several decades between about 10^5 and 10^{10}Hz, a region where considerable scatter of the data points is evident. See also the comparison between σ' data and fit for this region in Figures 2 and 3. If one defines NCL as a region of slope around 0 not exceeding ± 0.1, the region is, from the results of Figure 5b, about 2.2 decades in length and, of course, there is no non-zero-length region of zero slope present.

A CK1·SC composite model fits the present NCL region very well with only $\varepsilon_{D\infty}$, ρ_{C10}, A_{SC}, and γ_{SC} included as free parameters, leading to excellent S_F/PDRMS values of 0.003/0.04. Even without the ρ_{C10} parameter, the only part of the K1 model included above, a reasonably good C·SC fit of 0.014/0.10 was found. Earlier work has shown that a conductive-system model in series or parallel with a dielectric one can lead to NCL behavior over many decades, for example a CUN·SC model or one involving an effective-medium dielectric model in parallel with a CK1 conductive-system one.[22,40,42] Here, we see that just a C·SC model leads to an adequate fit of the NCL region, even though its three parameter estimates differ a bit from the corresponding ones in the model-B column of Table 2.

From the type-1 treatment of their 353 K CKN data, the authors of ref 25 concluded that, because their MC model, a conductive-system one involving translational motion of ions, led to good agreement with the data over most of the response region involving a σ' slope near 1, this was proof that CKN involves no NCL effect in the sense of Nowick, given that Nowick's definition of NCL held that it was unrelated to translational ionic transport and did not contribute to dc conductivity.[25] It might be mentioned that the MEMA model, which also involves response approaching 1 in the limit of high frequencies, might also lead to as good agreement with the 353 K data as that illustrated for the MC model.

It should be remembered, however, that the 353 K MC analysis took no account of electrode effects and probably did not involve a CNLS fit of the full data or even of that part extending up to the end of the apparent NCL region. Further, although two limiting values of ε_∞ are listed in ref 25, ones evidently not obtained from CNLS fitting, they are larger than either the 342 or 361 K values of Table 2. In addition, the ref-25 authors make no distinction between ε_∞ and the $\varepsilon_{D\infty}$ bulk dielectric parameter, one here involving induced dipoles and playing a crucial role in all parts of the full complex response, especially those including the NCL region as well as the vibratory one.

It would be interesting to see what results might be found if the above MC problems could be remedied while using an extended approach and full CNLS fitting. Until that happens, it seems most reasonable to postpone any conclusion that CKN involves no NCL of the restricted Nowick type. It is noteworthy, however, that, when it was found that the MC model was unable to represent data for other materials into the NCL region,[27] the authors there used an added empirical expression for this region that involved interacting ions moving in a double-well potential cage.

In contrast, the SC model not only represents much of the electrode polarization effects but also, and automatically, leads to excellent fitting of the NCL region as well, a possibility perhaps first demonstrated in 2002.[28] The SC therefore plays a double role here, one that involves mobile ions but not dc conductivity. Further, because low-frequency electrode polarization effects are associated with translational ionic motion, the SC-model's representation of NCL behavior is unlikely to involve caged ions. Finally, because the activation energy of A_{SC} is much smaller than that of σ_{C10}, as the temperature decreases, the C·SC part of the present composite model will eventually dominate, and γ_{SC} will increase toward a limit of 1, in agreement with observed low-temperature NCL behavior for many materials.

Acknowledgment. It is a pleasure to thank J. C. Dyre, R. F. Hamou, and G. P. Johari for valuable discussions and suggestions.

References and Notes

(1) Schrøder, T. B.; Dyre, J. C. *Phys. Rev. Lett.* **2008**, *101*, 025901.
(2) Davidson, D. W.; Cole, R. H. *J. Chem. Phys.* **1951**, *19*, 1484.
(3) Macdonald, J. R. *J. Chem. Phys.* **2002**, *116*, 3401.
(4) Macdonald, J. R. *Phys. Rev. B* **2005**, *71*, 184307.
(5) Macdonald, J. R. *J. Phys.: Condens. Matter* **2005**, *17*, 4369.
(6) Macdonald, J. R. *J. Phys.: Condens. Matter* **2006**, *18*, 629. On p 640, in the next-to-bottom line, replace $\rho_0\varepsilon_{D\infty}$ by $\rho_0\varepsilon_V\varepsilon_{D\infty}$. The word "imaginary" in the third line of p 634 should be replaced by "real".
(7) Macdonald, J. R. *J. Phys. Chem. B* **2007**, *111*, 7064. The symbol $K1\rho_\infty$ in the model designation appearing in section 5.2.2 should be written $K1\cdot\rho_\infty$.
(8) Macdonald, J. R. *J. Phys. Chem. B* **2008**, *112*, 13684.
(9) Macdonald, J. R. *J. Appl. Phys.* **1985**, *58*, 1955.
(10) Macdonald, J. R. *J. Appl. Phys.* **1985**, *58*, 1971.
(11) Macdonald, J. R. *J. Appl. Phys.* **1987**, *61*, 700.
(12) Dyre, J. C. *Phys. Lett.* **1985**, *108A*, 457.
(13) Dyre, J. C. *J. Appl. Phys.* **1988**, *64*, 2456.
(14) Dyre, J. C.; Schrøder, T. B. *Rev. Mod. Phys.* **2000**, *72*, 873.
(15) Macdonald, J. R. *J. Appl. Phys.* **1989**, *65*, 4845.
(16) Scher, H.; Lax, M. *Phys. Rev. B* **1973**, *7*, 4491.
(17) Macdonald, J. R. *Solid State Ionics* **2002**, *150*, 263. The symbol $\rho_{C1\infty}$ at the left side of the equation above Figure 6 on p 274 should be replaced by $\tau_{C1\infty}$.
(18) Lax, M.; Scher, H. *Phys. Rev. Lett.* **1977**, *39*, 781.
(19) Moynihan, C. T.; Boesch, L. P.; Laberge, N. L. *Phys. Chem. Glasses* **1973**, *14*, 122.
(20) Niklassson, G. A. *J. Appl. Phys.* **1989**, *66*, 4350.
(21) (a) Macdonald, J. R.; Potter, L. D., Jr. *Solid State Ionics* **1987**, *23*, 61. (b) Macdonald, J. R. *J. Computational Phys.* **2000**, *157*, 280. The newest Windows version, LEVMW, of the comprehensive LEVM fitting and inversion program can be downloaded at no cost by accessing http://jrossmacdonald.com. It includes an extensive manual and executable and full source code. More information about LEVM is provided at this internet address. All of the Macdonald works cited herein are available in PDF format for downloading from this address.
(22) Macdonald, J. R.; Ahmad, M. M. *J. Phys.: Condens. Matter* **2005**, *19*, 046215.
(23) Macdonald, J. R. *J. Phys. Chem. Solids* **2009**, *70*, 546.
(24) Parthun, M. G.; Johari, G. P. *J. Chem. Soc., Faraday Trans.* **1995**, *91*, 329.
(25) Funke, K.; Singh, P.; Banhatti, R. D. *Phys. Chem. Chem. Phys.* **2007**, *9*, 5582.
(26) Singh, P.; Banhatti, R. D.; Funke, K. *Phys. Chem. Glasses* **2005**, *46*, 241.
(27) Funke, K.; Banhatti, R. D. *Solid State Ionics* **2006**, *177*, 1551.
(28) Macdonald, J. R. *J. Non-Cryst. Solids* **2002**, *307*−*310*, 913.
(29) Kimball, J. C.; Adams, L. W., Jr. *Phys. Rev. B* **1973**, *18*, 5851.
(30) Funke, K.; Banhatti, R. D.; Cramer, C. *Phys. Chem. Chem. Phys.* **2005**, *7*, 157.
(31) Grassberger, P.; Procaccia, I. *J. Chem. Phys.* **1982**, *77*, 6281.
(32) Macdonald, J. R.; Phillips, J. C. *J. Chem. Phys.* **2005**, *122*, 074510.
(33) Strom, U.; Hendrickson, J. R.; Wagner, R. J.; Taylor, P. C. *Solid State Commun.* **1974**, *15*, 1871.
(34) Kenkel, S. W.; Macdonald, J. R. *J. Chem. Phys.* **1984**, *81*, 3215.
(35) Hamou, R. F.; Macdonald, J. R.; Tuncer, E. *J. Phys.: Condens. Matter* **2009**, *21*, 025904.
(36) Stromme Mattson, M.; Niklasson, G. A. *J. Appl. Phys.* **1999**, *85*, 2185.
(37) Elliott, S. R. *Europhys. Lett.* **1992**, *19*, 201.
(38) Lee, W. K.; Liu, J. F.; Nowick, A. S. *Phys. Rev. Lett.* **1991**, *67*, 1559.
(39) Macdonald, J. R. *Appl. Phys. A: Mater. Sci. Process.* **1994)** , *59*, 181.
(40) Macdonald, J. R. *J. Chem. Phys.* **2001**, *115*, 6192.
(41) Macdonald, J. R. *Phys. Rev. B* **2002**, *66*, 064305.
(42) Macdonald, J. R. *J. Appl. Phys.* **2003)** , *94*, 558.
(43) Dyre, J. C.; Maass, P.; Roling, B.; Sidebottom, D. J. *Rep. Prog. Phys.* **2009**, *72*, 046501.

JP9026095